Earth and Planetary Science Letters 558 (2021) 116762

Contents lists available at ScienceDirect

Earth and Planetary Science Letters

www.elsevier.com/locate/epsl

Primordial neon in high-^{3}He/^{4}He Baffin Island olivines

F. Horton [a,*], J. Curtice [a], K.A. Farley [b], M.D. Kurz [a], P.D. Asimow [b], J. Treffkorn [b], X.M. Boyes [b]

[a] Woods Hole Oceanographic Institution, United States of America
[b] California Institute of Technology, United States of America

ARTICLE INFO

Article history:
Received 7 October 2020
Received in revised form 11 December 2020
Accepted 11 January 2021
Available online xxxx
Editor: R. Dasgupta

Keywords:
primordial mantle
hotspot lavas
neon isotopes
noble gas geochemistry

ABSTRACT

Paleocene basaltic lavas exposed on Baffin Island have the highest ^{3}He/^{4}He found in any terrestrial igneous rocks and potentially contain the most pristine primordial mantle material exposed on Earth's surface. By vacuum-crushing large (1–3 g) olivine mineral separates, we extracted enough magmatic gas to obtain the first coupled helium, neon, and argon isotopic compositions of Baffin Island lavas. The five Baffin Island olivine samples have ^{3}He/^{4}He ranging from 36.2 ± 0.6 to 48.6 ± 1.3 (1σ) times the atmospheric ratio (Ra), overlapping with the highest known mantle values. Neon isotopic results fall on a mixing line between atmosphere and a high ^{20}Ne/^{22}Ne mantle endmember (with a maximum ^{20}Ne/^{22}Ne of 12.2). The slope of this mixing line is indistinguishable from that in subglacial Holocene glass from Iceland, but distinct from other hotspots and mid-ocean ridge basalt trends. This result supports the hypothesis that Baffin Island and Iceland lavas share a common high-^{3}He/^{4}He mantle component, despite the fact that recent paleogeographic reconstructions place the Iceland hotspot far from Baffin Island at the time of eruption (61 Ma). Our results also demonstrate that high-^{3}He/^{4}He mantle reservoirs have ^{3}He/^{22}Ne variability that either reflects ancient mantle heterogeneity or helium addition in the upper or lower mantle.

1. Introduction

Lavas erupted above volcanic hotspots (e.g., Iceland, Hawai'i, Samoa, and Galápagos) often have higher ^{3}He/^{4}He ratios than mid-ocean ridge basalts (MORB), which are produced by the melting of the upper mantle and typically have ^{3}He/^{4}He of ~8 Ra (where Ra is the atmospheric ^{3}He/^{4}He ratio of 1.384 × 10^{-6}). Helium in hotspot lavas is thought to be derived from a deep mantle reservoir with more primordial ^{3}He—because it is less degassed—than the convecting upper mantle (e.g., Allègre et al., 1983; Kurz et al., 1983). Hot mantle plumes may transport this high-^{3}He/^{4}He mantle material from the lower mantle to volcanic hotspots (e.g., Jackson et al., 2017). Paleocene basaltic lavas exposed on southeastern Baffin Island have the highest ^{3}He/^{4}He (up to 50 Ra: Stuart et al., 2003; Starkey et al., 2009) found in any terrestrial igneous rocks and arguably contain the most pristine primordial mantle material exposed on Earth's surface (Jackson et al., 2010). For this reason, the isotopic compositions of Baffin Island lavas provide unique insights into long-lived deep mantle reservoirs (e.g., Jackson et al., 2010; Rizo et al., 2016).

Baffin Island lavas and their conjugates along the west Greenland margin erupted at 61 Ma (Storey et al., 1998) and are generally considered to be part of the North Atlantic Igneous Province (Saunders et al., 1997) that extends from arctic Canada across Greenland to the British Isles. Speculation that they derived from the proto-Iceland hotspot is based on (i) their high MgO contents and similar latitude to Iceland (Clarke, 1968), (ii) some paleogeographic reconstructions that place a stationary Iceland plume in the Baffin Island vicinity at 70–90 Ma (Lawver and Müller, 1994), and (iii) elevated ^{3}He/^{4}He at both localities (Stuart et al., 2003). However, this is difficult to reconcile with the observation that Baffin Island lavas erupted long after the crust passed over the alleged hotspot and the fact that coeval eruptions attributed to the same plume erupted ~2000 km away in the British Isles (Saunders et al., 1997). Furthermore, Baffin Island and Iceland lavas have distinct lithophile element geochemical compositions. Although both magma suites formed from mixtures of depleted (low ^{87}Sr/^{86}Sr, low ^{187}Os/^{188}Os, high ^{143}Nd/^{144}Nd, and low incompatible trace element concentrations) and enriched (high ^{87}Sr/^{86}Sr, high ^{187}Os/^{188}Os, low ^{143}Nd/^{144}Nd, and higher incompatible trace element concentrations) mantle components, in detail the endmembers at the two localities are discrepant (Robillard et al., 1992; Kent et al., 2004; Willhite et al., 2019). So, the relationship between Baffin Island and Iceland mantle sources has remained uncertain. Here we report the first neon and argon isotopic results for

* Corresponding author.
E-mail address: horton@whoi.edu (F. Horton).

https://doi.org/10.1016/j.epsl.2021.116762
0012-821X/

the high-^{3}He/^{4}He Baffin Island lavas, which strengthen the links between Paleocene Baffin lavas and recent Iceland lavas. In a global geochemical context, these results also have implications for noble gas heterogeneity among high-^{3}He/^{4}He mantle reservoirs.

2. Materials and methods

Due to the absence of gas-rich submarine and subglacial glasses typically used for the analysis noble gases heavier than He, the only existing Baffin Island noble gas data are He measurements from olivine. To obtain coupled He, Ne, and Ar isotope data, we crushed olivine mineral separates to extract magmatic gases trapped in olivine-hosted inclusions. Five new picrite samples, collected in 2018, that contain olivines larger than 3 mm were selected from the lowermost subaerial lava flows on Durban Island, Padloping Island, and Cumberland Peninsula (see Appendix A). All samples were collected from cliff faces where they were well-shielded from cosmic rays. Olivine separates were handpicked from crushed and sieved (> 1 mm) size fractions of each sample, and then ultrasonically cleaned in ethanol. Matrix-free subsets (1.2–2.6 g) of the olivine separates were crushed under vacuum with a magnetically actuated metal sphere. To quantify any remaining gas and evaluate the presence of cosmogenic and radiogenic gases, crushed powder residue from each sample was then fused in vacuum.

For He-Ne-Ar analyses, gases extracted from olivines at intervals of 40 strokes of the crusher were purified on bulk Ti sponge and Zr-Fe-Al pellet getters. He and Ne were sorbed/desorbed on charcoal and nude stainless steel cryotraps, respectively, and were sequentially analyzed on a MAP 215-50 magnetic sector mass spectrometer at Woods Hole Oceanographic Institution. Procedural banks for ^{4}He were less than 5×10^{-12}, corresponding to <0.5% of the total gas released per sample and <5% per extraction step. Procedural blanks for ^{20}Ne were less than 4×10^{-12} cm^3 STP, which is 7–18% of the total ^{20}Ne released per sample and 13–95% per extraction step. Ar isotopes were measured on a Hiden Triple Filter quadrupole mass spectrometer in ion counting mode with blanks less than 4×10^{-9} cm^3 STP. After making blank and interference corrections, we normalized the results to in-house MORB glass and air standards, as described by Kurz et al. (2005, 2009). Fractions of the crush residue were subsequently fused in a double vacuum furnace at 1550 °C to extract any remaining gases, which were analyzed by the same methods described above.

In an attempt to characterize the Xe isotopic composition of sample PING18-H18, we crushed a different 4.8 g olivine separate under vacuum at California Institute of Technology. After cryofocusing at liquid nitrogen temperature on a glass finger and purification on a cycled SAES getter, we inlet the gases into a Helix-MC^{+10K} mass spectrometer and measured ^{124}Xe, ^{126}Xe, ^{128}Xe, ^{129}Xe, ^{130}Xe, ^{131}Xe, ^{132}Xe, ^{134}Xe, and ^{136}Xe. None of the four crush steps yielded anomalous air-normalized ^{n}Xe/^{130}Xe ratios beyond 2σ uncertainty. The key radiogenic isotope ratios (^{129}Xe/^{130}Xe, ^{134}Xe/^{130}Xe, and ^{136}Xe/^{130}Xe) deviate from the atmospheric ratios by less than 1.5%. For additional details about our Xe methods, see Appendix D.

3. Results

Total crushing yields per sample were 0.2–5.4 $\times 10^{-8}$ cm^3 STP ^{4}He/g, 1.4–4.8 $\times 10^{-11}$ cm^3 STP ^{20}Ne/g, and 0.8–24 $\times 10^{-8}$ cm^3 STP ^{40}Ar/g (Table 1). Based on the fusion yields, crushing extracted 3–58% of the He, 21–32% of the Ne, and 3–47% of the Ar in each sample (Tables 1 and B.1). ^{3}He/^{4}He ratios exceeded 35 Ra for every crushing extraction step, with a range of 36.2 ± 0.6 to 48.6 ± 1.3 Ra (1σ). Most of the sequential crush steps yielded consistent ^{3}He/^{4}He values within analytical uncertainty (see Appendix C for discussion about ^{3}He/^{4}He variability). There are two notable exceptions: The second extraction steps for PING18-H14 (48.6 ± 1.3 Ra) and RB18-H1 (38.9 ± 1.0 Ra). Although these crushing steps yielded little gas (<5 $\times 10^{-10}$ cm^3 STP ^{4}He/g), both had higher ^{3}He/^{4}He and ^{20}Ne/^{22}Ne ratios than their respective prior extractions, indicating a greater proportion of non-radiogenic gas.

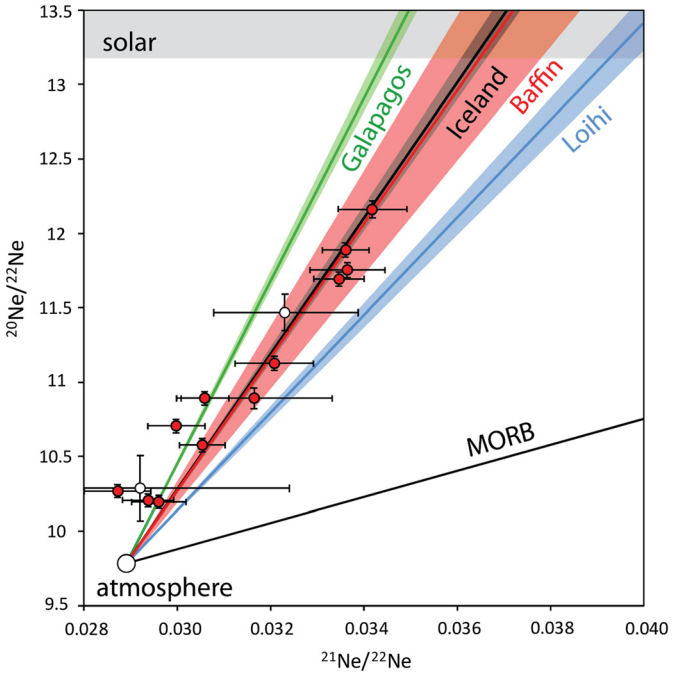

Fig. 1. Neon extracted from Baffin Island olivines (red data points) and West Greenland olivine-hosted melt inclusions (white: Péron et al., 2018) falls on a mixing line between high ^{20}Ne/^{22}Ne mantle and atmosphere. This trend is distinct from Fernandina/Galápagos (green: Kurz et al., 2009; Péron et al., 2016) and Loihi (blue: Valbracht et al., 1997) data, but indistinguishable from subglacial volcanic glass from Iceland (black: Mukhopadhyay, 2012). Best-fit lines are fixed to the atmospheric ratios and the shaded regions represent 2 standard error. The solar value of 13.36 ± 0.18 (2σ) is from Heber et al. (2012).

The ^{20}Ne/^{22}Ne and ^{21}Ne/^{22}Ne for each extraction step significantly exceeded the atmospheric ratios (9.8 and 0.029, respectively). Ne fusion analyses are isotopically indistinguishable from atmosphere, but are close to detection limits. In Ne three-isotope space, all except two crush analyses fall on a linear mixing line with atmosphere (Fig. 1). This line intersects Ne-B (^{20}Ne/^{22}Ne = 12.7; Moreira and Charnoz, 2016) and solar (^{20}Ne/^{22}Ne = 13.36; Heber et al., 2012) at ^{21}Ne/^{22}Ne of 0.0354 ± 0.001 and 0.0368 ± 0.001, respectively. The slope of the correlation in Ne three-isotope space is identical within error to the slope established for well-studied Iceland glass (Mukhopadhyay, 2012). Two lava samples from West Greenland (thought to be conjugates of Baffin Island eruptions) have olivine-hosted melt inclusions (^{3}He/^{4}He = 31–35 Ra) containing neon that also fall along this mixing line (Péron et al., 2018).

^{40}Ar/^{36}Ar crushing results range from 327 to 3,933 and correlate with ^{20}Ne/^{22}Ne (Fig. 2a); a similar trend is observed in subglacial glass from Iceland. Although ^{3}He/^{36}Ar also correlates with ^{40}Ar/^{36}Ar and ^{3}He/^{22}Ne also correlates with ^{20}Ne/^{22}Ne, there is more scatter in these trends and both differ from the slopes in Iceland subglacial glass data. Assuming all the measured ^{36}Ar is due to air contamination with a ^{40}Ar/^{36}Ar ratio of 295.5, two samples (PING18-H18 and DURB18-H8) contained ~65% air and had ^{4}He/^{40}Ar* (where ^{40}Ar* is the contamination-corrected value) ranging from 0.15–0.51, whereas the other samples contained ≥80% air contamination and had ^{4}He/^{40}Ar* of 0.08–0.84.

Table 1
Noble gas olivine crushing results. See Table B.1 for fusion experiments on the crush residue.

	mass (g)	^{4}He (10^{-9} cm^3/g)	^{3}He/^{4}He (Ra)	1σ	^{20}Ne (10^{-11} cm^3/g)	^{21}Ne/^{22}Ne	1σ	^{20}Ne/^{22}Ne	1σ	^{40}Ar (10^{-8} cm^3/g)	^{40}Ar/^{36}Ar	1σ
DURB18-H8	2.47											
Crush 1		7.59	45.0	1.1	1.34	0.0306	0.0005	10.89	0.04	2.76	1471	27
Crush 2		7.98	43.9	1.0	0.50	0.0321	0.0008	11.13	0.05	1.76	2628	127
Total		15.57			1.83					4.52		
DURB18-H10	1.24											
Crush 1		1.27	36.2	0.6	1.40	0.0305	0.0005	10.58	0.05	0.82	401	2
PING18-H14	2.24											
Crush 1		1.24	37.0	1.0	2.16	0.0296	0.0006	10.20	0.04	2.64	503	4
Crush 2		0.38	48.6	1.3	0.88	0.0300	0.0006	10.71	0.04	0.47	397	2
Crush 3		0.11	38.3	1.2	0.61	0.0287	0.0007	10.27	0.04	0.38	442	2
Total		1.73			3.65					3.50		
PING18-H18	2.60											
Crush 1		13.84	43.4	1.1	1.86	0.0335	0.0005	11.69	0.05	9.41	2597	70
Crush 2		31.33	41.9	0.6	1.82	0.0336	0.0005	11.89	0.05	8.74	3933	218
Crush 3		5.62	42.5	0.7	0.76	0.0336	0.0008	11.75	0.05	3.74	3897	97
Crush 4		2.94	42.2	0.7	0.36	0.0342	0.0007	12.16	0.06	2.12	3779	80
Total		53.74			4.79					24.01		
RB18-H1	1.47											
Crush 1		1.47	36.1	0.5	2.46	0.0294	0.0006	10.21	0.04	1.80	327	5
Crush 2		0.20	38.9	1.0	0.34	0.0316	0.0017	10.89	0.07	0.27	338	2
Total		1.67			2.79					2.06		

We did not measure anomalous air-normalized xenon isotopic ratios beyond 2σ uncertainty. This result is consistent with air contamination of sufficient magnitude to preclude detection of an anomalous Baffin Island mantle Xe component. See Appendix D for detailed Xe results.

4. Discussion

Ne in Baffin Island olivines bears a striking isotopic resemblance to that in subglacial Holocene glass from Iceland. Both datasets define comparable mixing lines between mantle and atmosphere (Fig. 1: Harrison et al., 1999; Moreira et al., 2001; Füri et al., 2010; Mukhopadhyay, 2012), although some Iceland data extend to higher ^{20}Ne/^{22}Ne values (i.e., they are less air contaminated) than the maximum obtained from Baffin Island olivine samples. Despite the overlap in Ne isotopes, the He isotope ratios of these two suites are clearly different: The Iceland array is defined by gas extractions from a sample with a ^{3}He/^{4}He ratio of 17 Ra (Mukhopadhyay, 2012), whereas the Baffin Island olivines yielded ratios of 36.2 $\pm$ 0.6 to 48.6 $\pm$ 1.3 Ra. Within analytical uncertainty, the highest value in the new data overlaps with the highest published terrestrial igneous value, which was also obtained from Baffin Island olivines (49.8 $\pm$ 0.7 Ra: Starkey et al., 2009). Notably, the slope of the Baffin trend in Ne isotopic space is distinct from the steeper Galápagos (Kurz et al., 2009; Péron et al., 2016) and shallower Loihi (Valbracht et al., 1997) trends. Kola carbonatites (Marty et al., 1998; Yokochi and Marty, 2004), Samoa xenoliths (Poreda and Farley, 1992), and Réunion lavas (Staudacher et al., 1990) contain Ne with air-mixing slopes mostly intermediate between the Loihi and MORB lines (Moreira et al., 1998). Critically, there was no systematic increase in ^{21}Ne/^{22}Ne or systematic decrease in ^{3}He/^{4}He during sequential crushing extraction steps in any sample. Such trends would have indicated contamination by a matrix-hosted component of post-magmatic gas with high (nucleogenic) ^{21}Ne/^{22}Ne and low (radiogenic) ^{3}He/^{4}He. Such a component may be present, but it was apparently not extracted by the crushing procedure. Therefore, the Ne extracted by crushing is probably a near-binary mixture of atmosphere and a mantle component indistinguishable from that measured in subglacial Iceland glass. This observation has implications for understanding Iceland hotspot evolution, the origins of olivine-hosted noble gases, and Ne systematics in mantle.

4.1. Hotspot implications

Baffin Island and Iceland lavas—and presumably the mantle reservoir(s) from which they derived—share a common Ne component that is distinct from other hotspots and MORB. This observation is most simply explained if Baffin Island lavas contain Ne from the proto-Iceland mantle plume. This hypothesis is supported by the fact that Iceland and Baffin Island lavas both contain a putative primitive mantle component defined by high ^{3}He/^{4}He ratios and radiogenic isotopes (Jackson et al., 2010). Furthermore, there are no long-lived mantle hotspots in the North Atlantic other than Iceland that could have fed the Baffin Island magmatism.

The proto-Iceland plume may not have been directly beneath Baffin Island at the time of eruption. Baffin Island and West Greenland eruptions began between 61.3 Ma and 60.9 Ma and lasted less than 1 Myr (Storey et al., 1998). Plate reconstructions and plume motions place the hotspot beneath central (Forsyth et al., 1986; Lawver and Müller, 1994) or eastern Greenland (White and McKenzie, 1989; Torsvik et al., 2015; Steinberger et al., 2019) at 60 Ma (Fig. 3). This implies that the proto-Iceland plume may have been 500–1000 km away when Baffin Island lavas erupted. One possible explanation is that the proto-Iceland hotspot implanted noble gases into the mantle lithosphere as it passed beneath what is now Baffin Island at 80–70 Ma; magmatism associated with continental rifting during the opening of Davis Strait might have then tapped this fossil noble gas reservoir. In such a scenario, it is difficult to explain the hotspot-like mantle potential temperatures in excess of 1500 °C recorded in Baffin Island lavas (Willhite et al., 2019), including our samples (according to PRIMELT3: Herzberg and Asimow, 2015).

Alternatively, bifurcation of a proto-Iceland plume could explain volcanism far from the center of the hotspot. 3-D numerical modeling indicates that the passage of continental lithosphere (in this case Greenland) over a surfacing diapiric plume head can cause simultaneous and asymmetric melting on either side of the litho-

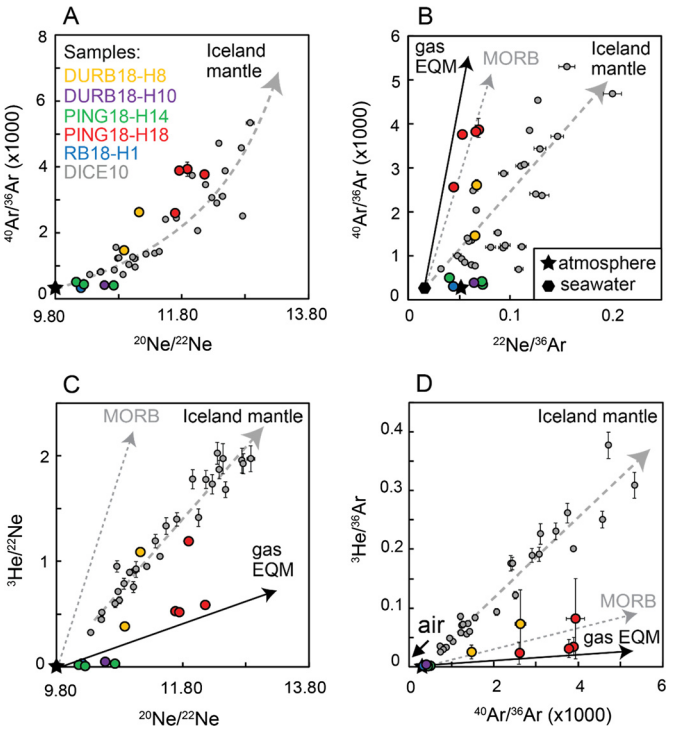

Fig. 2. Baffin Island olivine He-Ne-Ar isotopic results in comparison to subglacial volcanic glass from Iceland (DICE10: Mukhopadhyay, 2012). Comparable Ne and Ar isotopic trends (panel A) may indicate that Baffin Island and Iceland lavas share a common mantle source. If so, and if noble gas elemental ratios of sources are faithfully inherited by primitive lavas, then there is evidence of elemental fractionation processes in the Baffin Island olivine and in Icelandic glass interelement ratios. In Baffin Island olivine, Ne is depleted relative to Ar (panel B) and He is depleted relative to both Ne (panel C) and Ar (panel D). Stars denote atmospheric ratios. MORB mixing arrays defined by Raquin et al. (2008) and Mukhopadhyay (2012) are shown for reference. The black line shows the maximum theoretical closed-system equilibrium fractionation between a gas phase and Iceland-like basaltic melt. The difference in slope between the trend defined by the Iceland data (bold grey dashed line) and gas in equilibrium with basaltic melt of that composition ("gas EQM") is defined by ratios of solubilities of the different gases in the melt (based on solubilities at 1500 °C: Jambon et al., 1986). Note that, in panel B, trendlines intersect seawater ratios rather than atmospheric ratios (after Mukhopadhyay, 2012). Error bars are shown unless they are smaller than the symbols.

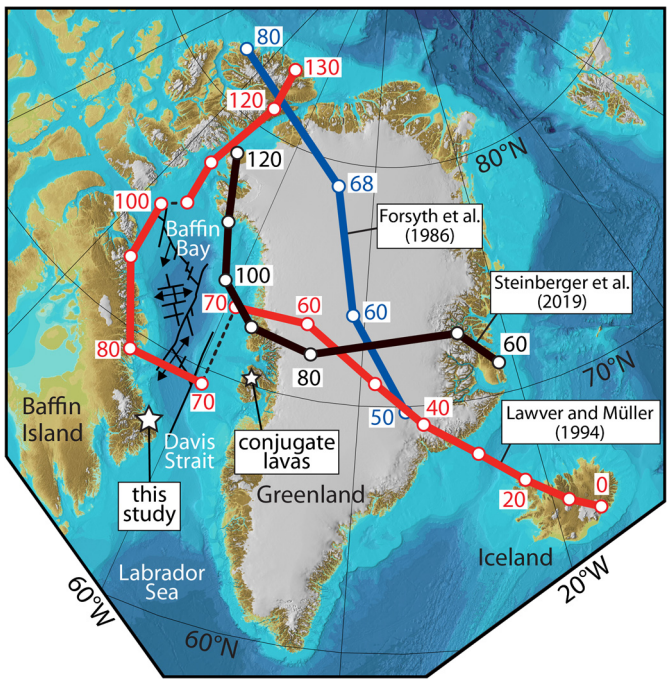

Fig. 3. Projected Iceland hotspot tracks from three studies (Forsyth et al., 1986; Lawver and Müller, 1994; Steinberger et al., 2019). The 61 Ma Baffin Island lavas sampled in this study erupted far from projected hotspot location for that time. Note that Baffin Bay and Davis Strait opened since then; transform faults and spreading ridges in Baffin Bay (Oakey and Chalmers, 2012) are plotted to show the direction of rifting. The shaded relief map is modified from Jakobsson et al. (2012).

spheric keel (Manglik and Christensen, 2006). This might explain lateral flow of proto-Iceland plume material beneath thick lithosphere (Saunders et al., 1997) or along a corridor of thinned Greenland lithosphere (Nielsen et al., 2002; Steinberger et al., 2019). Under these circumstances, it is surprising that Baffin Island lavas lack isotopic evidence of lithospheric contamination (Kent et al., 2004; Lass-Evans, 2004; Jackson et al., 2010), unlike East Greenland flood basalts (e.g., Hansen and Nielsen, 1999) that probably erupted much nearer to the center of the plume (Steinberger et al., 2019). These geochemical and geophysical constraints seem to necessitate—if Baffin Island is sourced from the proto-Iceland plume—that hotspot material either (1) resided at the base of the lithosphere for tens of millions of years without contamination or (2) briefly flowed westward shortly after the proto-Iceland mantle plume head reached the base of the Greenland lithosphere.

4.2. Olivine-hosted noble gases

The vast majority of mantle-derived heavy noble gas measurements have been obtained by crushing vesicular submarine or subglacial basalt glass. The few attempts to characterize these gases in olivine have met with limited success (e.g., Poreda and Farley, 1992; Farley and Craig, 1994; Dixon et al., 2000; Sumino et al., 2006; Jackson et al., 2009; Péron et al., 2018), so this dataset provides unique insights into olivine-hosted noble gases.

In Baffin Island olivine, $^{20}Ne/^{22}Ne$ correlates positively with $^{40}Ar/^{36}Ar$ (Fig. 2A) along a trend that overlaps the range observed in subglacial Iceland glass (Mukhopadhyay, 2012). This is broadly consistent with binary mixing between mantle- and atmosphere-like noble gases. This relationship breaks down, however, when we compare elemental abundance ratios. The Baffin Island analyses with the greatest mantle component have $^{22}Ne/^{36}Ar$ (Fig. 2B), $^{3}He/^{22}Ne$ (Fig. 2C), and $^{3}He/^{36}Ar$ (Fig. 2D) ratios lower than corresponding Iceland analyses. If we assume that the Iceland data are representative of primary Baffin Island magma compositions, then Baffin Island olivines exhibit signs of Ne depletion relative to Ar and He depletion relative to both Ne and Ar.

Magmatic degassing prior to gas entrapment in Baffin Island olivines and/or post-entrapment modification could account for the observed elemental fractionation. During magmatic degassing, noble gas fractionation is typically controlled by the competing effects of solubility and kinetics (e.g., Tucker et al., 2018) because noble gas diffusivities (Lux, 1987) and solubilities (Jambon et al., 1986) in basaltic melts decrease with atomic size. Deviation of Baffin Island data from the Iceland trendlines in Fig. 2 approaches the maximum possible closed-system solubility-controlled fractionation, as defined by a difference in slope proportional to the ratio of He:Ne:Ar solubilities (14.3: 4.4: 1) at 1500 °C (Jambon et al., 1986). This is consistent with a scenario in which olivines trapped exsolved gases in near-equilibrium with Iceland-like primary magmas. It also suggests that the volatiles in olivine-hosted fluid inclusions record the composition of an exsolved volatile phase *prior* to open-system degassing. Subsequent diffusive loss of He from olivine-hosted fluid inclusions (e.g., Horton et al., 2019) cannot be ruled out, but is not required by these results.

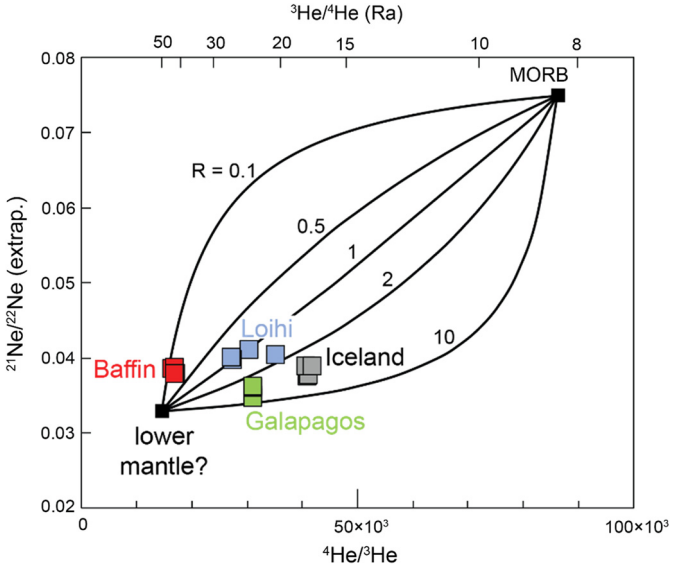

Fig. 4. Relations between ^{4}He/^{3}He and ^{21}Ne/^{22}Ne (extrap.) illustrate that binary mixing between (theoretical) lower mantle and MORB-like mantle components with fixed isotopic and elemental ratios fails to explain the He-Ne isotopic variability measured in high-^{3}He/^{4}He hotspot lavas. ^{21}Ne/^{22}Ne (extrap.) = [0.029 + 4 × (^{21}Ne/^{22}Ne−0.029)/(^{20}Ne/^{22}Ne−9.8)] and represents an extrapolation from atmosphere to ^{20}Ne/^{22}Ne = 13.8 (after Kurz et al., 2009). Black curves show mixing between the two end members for given values of R = (^{3}He/^{22}Ne$_{MORB}$)/(^{3}He/^{22}Ne$_{lower\text{-}mantle}$). Baffin Island data from this study is compared with Fernandina/Galápagos (Péron et al., 2016), Iceland subglacial glass (Mukhopadhyay, 2012), and Loihi (Valbracht et al., 1997). For clarity, only four representative analyses (those with the highest ^{20}Ne/^{22}Ne) from each dataset are shown. Uncertainties are smaller than the symbols.

4.3. He-Ne relationships in the mantle

The decay of uranium and thorium produces radiogenic ^{4}He and nucleogenic Ne isotopes, so we might expect that, globally, mantle ^{3}He/^{4}He would correlate with slope in Ne isotopic space (e.g., Honda et al., 1993; Farley and Neroda, 1998). If so, Ne measurements from Baffin Island (up to 50 Ra: Stuart et al., 2003; Starkey et al., 2009), Hawai'i (up to 32 Ra: Kurz et al., 1983), and Samoa (up to 34 Ra: Jackson et al., 2007) should fall to the left of the Galápagos trend defined by samples with maximum ^{3}He/^{4}He ratios ∼30 Ra. Instead, Baffin Island lavas that have the highest terrestrial magmatic ^{3}He/^{4}He ratios do not have similarly extreme Ne isotopic compositions (Fig. 1). For this reason, global isotopic variability in He and Ne cannot be explained by binary mixing between a single homogenous lower mantle component and a single homogenous MORB source with fixed elemental compositions (Fig. 4).

The ^{3}He/^{22}Ne ratio is useful for understanding mantle evolution because neither ^{3}He nor ^{22}Ne is produced in the mantle in significant quantities over geologic time. Using the methods described by Tucker and Mukhopadhyay (2014) and Dygert et al. (2018), we calculate that the time-integrated ^{3}He/^{22}Ne composition of the Baffin Island mantle source is 7.3–8.6 (based on sample PING18-H18). This is similar to MORB mantle (7.5 ± 1.2: Dygert et al., 2018) and intermediate between depleted mantle (>10) and primordial materials (<2: Tucker and Mukhopadhyay, 2014). Baffin Island mantle ^{3}He/^{22}Ne is notably higher than Iceland and Galapagos mantle (both ∼2) and significantly above the global ocean island basalt mantle range (3.5 ± 2.4: Dygert et al., 2018).

Our determination of higher time-integrated ^{3}He/^{22}Ne in Baffin Island mantle than in ocean island basalt mantle poses a problem for models in which high ^{3}He/^{4}He material derives from deep ancient reservoirs with low ^{3}He/^{22}Ne, such as mantle domains that survived the moon-forming giant impact (Tucker and Mukhopadhyay, 2014) or otherwise non-degassed, long-isolated mantle domains (Dygert et al., 2018). It also precludes derivation of high-^{3}He/^{4}He material from the core (Bouhifd et al., 2020), assuming that the addition of core gases to the mantle does not fractionate the He/Ne ratio. The inferred high Baffin source ^{3}He/^{22}Ne seems to necessitate mechanisms other than magma ocean in-gassing (Tucker and Mukhopadhyay, 2014) and kinematic fractionation—driven by faster He diffusion—beneath spreading ridges domains (Dygert et al., 2018).

Given the proximity of Baffin Island lavas to—and probable derivation from—the proto-Iceland plume, it is especially difficult to reconcile the Ne isotopic similarities and ^{3}He/^{4}He differences at these two localities. Even though MORB has a higher ^{3}He/^{22}Ne ratio (∼7.5: Dygert et al., 2018) than the Iceland hotspot (∼2: Mukhopadhyay, 2012), mixing of MORB-like gases into a hotspot reservoir strongly affects the He *and* Ne isotopic ratios. For example, a mixture of 65% Baffin Island (^{3}He/^{4}He of 50 Ra, ^{21}Ne/^{22}Ne of 0.035, and solar nebula-like ^{3}He/^{22}Ne of 1.5) and 35% MORB (8 Ra) gases produces a ^{3}He/^{4}He ratio comparable to Iceland subglacial glass (18 Ra) and an unrealistically high ^{21}Ne/^{22}Ne ratio (0.0385). Thus, mixing with MORB source fails to explain our Baffin Island results unless the Iceland plume had an initially distinct Iceland-like (low ^{21}Ne/^{22}Ne) source region that coincidentally mixed with precisely enough MORB source to be indistinguishable from Baffin-like (higher ^{21}Ne/^{22}Ne) material. Nor can binary mixing between a MORB-like and a high-^{3}He/^{4}He primordial mantle endmember explain the compositional variability among Iceland lavas themselves (Füri et al., 2010).

We propose three scenarios that satisfy the Baffin Island and Iceland noble gas constraints. First, Iceland results can be explained by the addition of MORB-like or crustal He (but not Ne) to a proto-Iceland hotspot with an initial ^{3}He/^{4}He ratio of ∼50 since 60 Ma. This could explain ^{3}He/^{22}Ne heterogeneity among lavas from individual hotspots and among hotspot lavas globally. Second, Baffin and Iceland lavas could have derived from a mantle source region with uniform Ne isotopic ratios and heterogeneous ^{3}He/^{22}Ne. This could be a manifestation of the ^{3}He/^{4}He and μ^{182}W temporal variability observed in Iceland hotspot lavas (Mundl-Petermeier et al., 2019), which is attributed to geochemically textured ancient mantle domains. Third, diffusion of He across the core-mantle boundary (e.g., Porcelli and Halliday, 2001) could impart a high-^{3}He/^{4}He signature on mantle hotspot source regions and explain the fractionation of He from Ne. In this case, the differences between Baffin Island and Iceland mantle sources could reflect the addition of different amounts of core-derived He. Although we cannot distinguish among these scenarios, our Baffin Island results are strong evidence for He and Ne elemental fractionation in hotspot mantle.

CRediT authorship contribution statement

F. Horton: Conceptualization, Formal analysis, Funding acquisition, Methodology, Supervision, Visualization, Writing – original draft. **J. Curtice:** Formal analysis, Investigation. **K.A. Farley:** Conceptualization, Funding acquisition, Investigation, Methodology, Resources, Supervision. **M.D. Kurz:** Investigation, Resources, Writing – review & editing. **P.D. Asimow:** Conceptualization, Funding acquisition, Supervision, Writing – review & editing. **J. Treffkorn:** Formal analysis, Investigation, Writing – original draft. **X.M. Boyes:** Formal analysis, Investigation.

Declaration of competing interest

The authors declare that they have no known competing financial interests or personal relationships that could have appeared to influence the work reported in this paper.

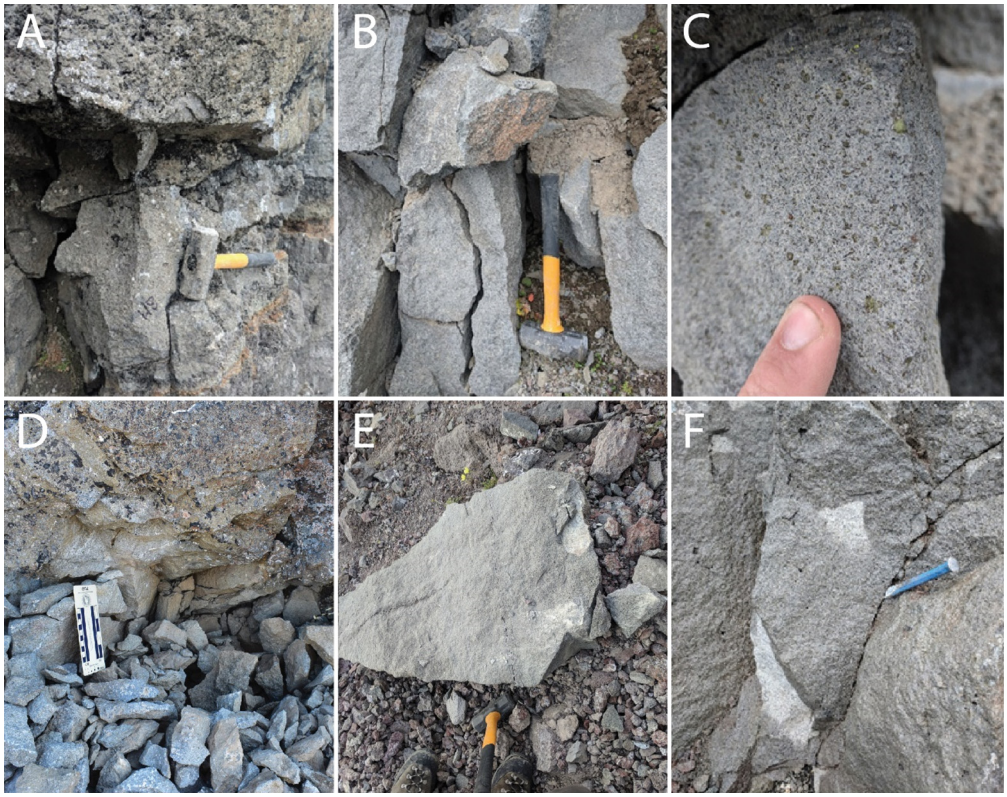

Fig. A.1. Field photographs of the Baffin Island samples. Sample DURB18-H8 was collected immediately above a palagonite-rich flow top (A); sample DURB18-H10 is from the interior of a flow (B) and contains abundant phaneritic olivines (C); sample PING18-H14 was retrieved from a deep recess in an outcrop (D); sample PING18-H18 is from a slab that recently fell from the cliff face (E); and sample RB18-H1 is from a vertical outcrop (F). (For interpretation of the colors in the figure(s), the reader is referred to the web version of this article.)

Acknowledgements

The National Science Foundation (award #1911699) funded this research. The Woods Hole Oceanographic Institution (WHOI) Andrew W. Mellon Foundation Endowed Fund for Innovative Research and a National Geographic Society grant (#CP4-144R-18) supported fieldwork activities. The WHOI noble gas lab was supported by NSF OCE #1259218 and WHOI. We thank Maryse Mahy of the Parks Canada Nunavut Field Unit, the Qikiqtani Inuit Association, and the Nunavut Research Institute for their assistance and cooperation. Victoria Hooton provided invaluable help with mineral separation. Two anonymous reviews improved the manuscript.

Appendix A. Sample descriptions

DURB18-H8 (67.08585° N, 62.22996° W, elevation 468 m): This sample is a vesicular pilotaxitic picrite with a plagioclase microlite groundmass collected from the base of the second subaerial lava flow on SW Durban Island. Olivines range in size from <1 mm to 4 mm. The orange palagonite-rich top of the previous flow is visible in Fig. A.1A. The sample was collected beneath an overhang from the section labeled "H8".

DURB18-H10 (67.08585° N, 62.22939° W, elevation 470 m): This sample is from the interior of the flow immediately above DURB18-H8, where vesicles are absent and the groundmass—composed of intergrown plagioclase and augite—is coarser. Two pieces were collected to the left of the hammer in Fig. A.1B. Fresh subhedral to anhedral phaneritic olivines were abundant (Fig. A.1C). Euhedral olivines range in size from <1 mm to 3 mm.

PING18-H14 (67.18033° N, 62.40622° W, elevation 420 m): This sample is from below the ridgeline on the NE tip of Padloping Island and contains coarse lath-shaped and subhedral olivines amid phaneritic intergrowths of plagioclase and augite. We pulled adjacent samples from a recess in a steep outcrop (Fig. A.1D) where they were well shielded from cosmic rays. Olivines range in size from <1 mm to 3 mm. Slumping along steep normal faults in this area prevented precise stratigraphic comparisons, but the Padloping Island samples are further above the pillow sequence and therefore presumably stratigraphically higher than the Durban Island samples.

PING18-H18 (67.17317° N, 62.40268° W, elevation 533 m)**:** This picrite is from the northeastern tip of Padloping Island, at the base of vertical northeast-facing cliffs. It is petrologically similar to PING18-H14. The sample is from a ∼2 m tall slab (Fig. A.1E) that fell away from the lower portions of a thick (∼20 m) subaerial flow. The slab exhibited no discoloration or weathering, so we suspect that the sample was displaced recently and experienced little cosmic ray bombardment. Olivines range in size from <1 mm to 4 mm. The PING18-H18 olivine separate was unique in that a subset of the olivines contained abundant spherical fluid inclusions up to 100 µm in diameter while lacking inclusions of other types (Fig. A.2).

RB18-H1 (67.04101° N, 62.11762° W, elevation 524 m)**:** This pilotaxitic picrite is from a vertical outcrop exposing the upper portion of a lava flow on the northernmost part of Cumberland Peninsula, overlooking Durban Harbor. The sampled flow is at least four flows above the submarine-subaerial transition. Olivines range in size from <1 mm to 3 mm. The blue chisel in Fig. A.1F was driven into the outcrop as imaged to extract the material shown in the center of the photograph.

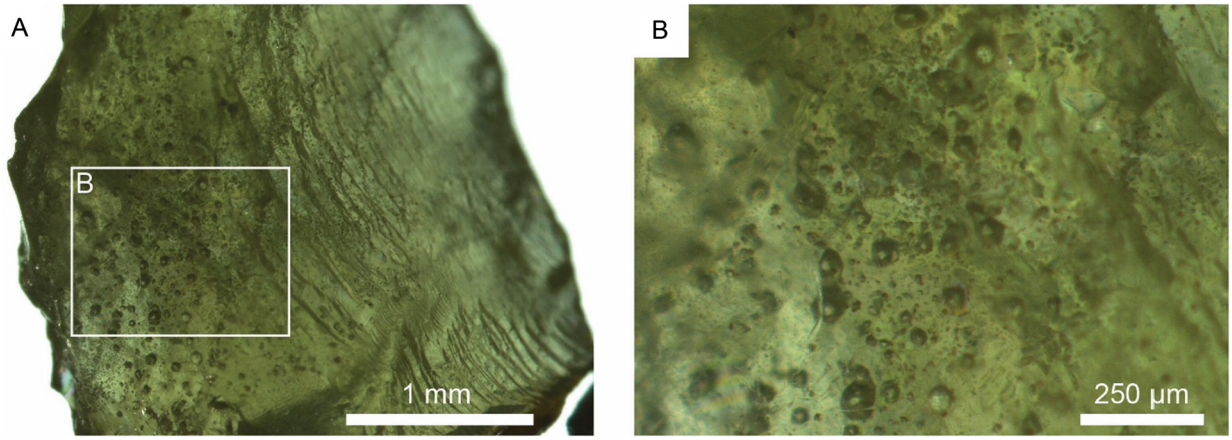

Fig. A.2. Photomicrographs of a representative fluid inclusion-rich olivine from sample PING18-18 taken on a stereoscopic microscope. Panel (B) is an image taken at higher magnification of the inset region outlined in panel (A).

Appendix B. Fusion results for crush residue

Table B.1
Noble gas results for fusion experiments on crush residue.

	mass (g)	^{4}He ($\frac{10^{-9}\ cm^3}{g}$)	$\frac{^3He}{^4He}$ (Ra)	1σ	^{20}Ne ($\frac{10^{-11}\ cm^3}{g}$)	^{40}Ar ($\frac{10^{-8}\ cm^3}{g}$)
DURB18-H8	0.22341	5.48	33.0	0.7	1.22	1.60
DURB18-H10	0.24476	3.55	11.6	0.4	1.90	2.29
PING18-H14	0.23643	14.90	3.8	0.1	1.86	2.36
PING18-H18	0.24963	9.80	35.5	0.6	2.93	6.77
RB18-H1	0.25372	3.47	10.5	0.3	1.58	3.42

Appendix C. Helium isotopic variability

The purpose of crushing is to preferentially release inclusion-hosted mantle gases. ^{3}He/^{4}He ratios can decrease with progressive crushing because the extracted gases can have a growing fraction of matrix-bound radiogenic ^{4}He. So, it is surprising that we measured the highest ^{3}He/^{4}He (48.6 Ra) during the second extraction step for sample PING18-H14. Although increases in ^{3}He/^{4}He across crushing steps can indicate the release of cosmogenic ^{3}He from the olivine lattice, four lines of reasoning suggest that this is not the case for PING18-H14: (1) the sample was well shielded from cosmic rays, (2) the ^{3}He/^{4}He decreased to 38.3 Ra during the third extraction, (3) the second extraction had mantle-like high ^{20}Ne/^{22}Ne compared to the other extraction steps, and (4) the fusion measurement yielded ^{3}He/^{4}He lower than crushing, which argues against the presence of cosmogenic helium. Thus, we conclude that the high ^{3}He/^{4}He reflects the mantle He isotopic compositions rather than any contribution from cosmogenic ^{3}He.

Intrasample ^{3}He/^{4}He variability could be caused by variable contributions of radiogenic ^{4}He or magma mixing/assimilation pro-

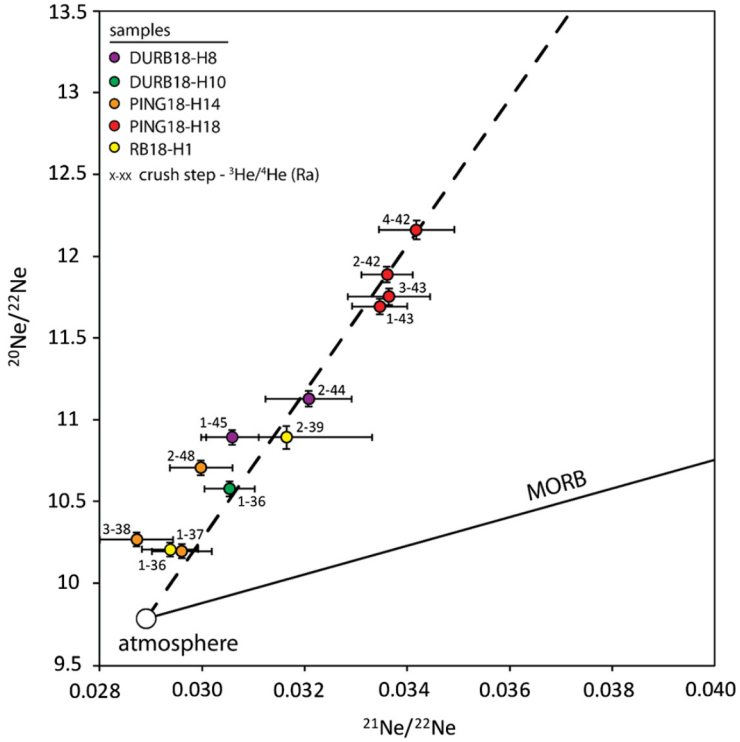

Fig. B.1. Neon isotopic results color-coded by sample. For reference, the best-fit line through the crushing results is shown as a dashed line. Note that the crush step and ^{3}He/^{4}He (Ra) results for individual analyses are listed next to each symbol.

cesses prior to eruption. Minimal $^{3}He/^{4}He$ variability is observed in the gas-rich samples (DURB18-H8 and PING18-H18), which is consistent with the contamination of isotopically homogenous He in each sample by radiogenic ^{4}He. However, in situ ^{4}He production in Baffin Island olivine lattices was probably minimal. The U and Th concentrations in Baffin Island lavas are <1 ppm (Lass-Evans, 2004) and the olivine-melt partition coefficients for these elements are very small ($D_{U\text{-}melt}$ and $D_{Th\text{-}melt}$ are approximately 6×10^{-6} and 1×10^{-6}, respectively: Blundy and Wood, 2003). Assuming olivine U and Th concentrations in equilibrium with the melt, ^{4}He production over 61 Myr would be $<5 \times 10^{-11}$ $^{4}He/g$ ($<4\%$ of the total He extracted from each sample), some fraction of which was retained in the crush residue. This is too little radiogenic ^{4}He to explain the observed $^{3}He/^{4}He$ variability, but it is possible that ^{4}He from melt inclusions—or produced in the basaltic matrix and implanted in olivine rims—is a major cause of $^{3}He/^{4}He$ variability.

Appendix D. Xenon methods and results

Xe standardization

Our primary Xe calibration is a cylinder and pipette system ("air standard") that delivers 1.849 ± 0.02 pcc of atmospheric Xe. This amount of Xe is inadequate for routine calibration of the Helix-MC, so a secondary Xe standard (XeStd) was prepared. This cylinder was filled with commercial Xe gas. The amount delivered by each pipette shot and the Xe isotopic composition of XeStd were determined by cross-calibration against the air standard. We are thus explicitly assuming that the air standard is unfractionated atmospheric Xe (Fig. D.1). We assumed a standard atmospheric composition of 87 ppm Xe and use the atmospheric isotopic abundances tabulated in Table D.1.

Xe gas from two replicates (each of either 4 or 6 shots) of the air standard was analyzed on the Helix-MC^{+10K} as described below. A line blank was processed in the same way. After blank correction, these four standard runs were used to calibrate sensitivity for each of the Xe isotopes. Sensitivity varies from detector to detector because of differences in gain and the exact measurement point on the mass spectrometer peak. Typical sensitivity for the Xe isotopes is about 550 cps/pcc. Nine replicate aliquots of the XeStd were analyzed in the same analytical session and in the same manner. The count rates on each isotope were averaged, and the mass spectrometer sensitivities for each isotope implied by the air standard runs were used to invert for the absolute abundance of each isotope in XeStd. Using a signal-weighted mean of the $^{n}Xe/^{132}Xe$ ratios normalized to air, these measurements indicate XeStd delivers 16.69 pcc STP of total Xe that is mass fractionated from atmospheric xenon by -1.047% per AMU (Fig. D.2). This mass fractionation estimate was used to correct each isotopic abundance in XeStd. The estimated uncertainty propagated to the amounts of each isotope in XeStd is at most 0.6%. See Table D.2.

Sample and standard gas preparation procedure

Gas introduced either from the crusher or from the standard pipette was cryofocused on a glass finger held at liquid nitrogen temperature for 500 seconds. With the liquid nitrogen still in place, the noncondensable gases were pumped to a turbomolecular pump for five minutes. After isolating from the pump, the liquid nitrogen was removed and the glass finger was heated resistively to above room temperature. The liberated Xe was then purified of active species on an SAES getter cycled from about 300 °C to room temperature over a ten-minute period.

Purified Xenon (plus residual Kr) was introduced into a Helix-MC^{+10K} mass spectrometer for analysis. Measurements were made in pulse counting mode on the 5 CDD detectors. In the first peak group, masses 124, 126, 128, 132, and 136 were measured in L2, L1, AX, H1, and H2, respectively. After a magnetic jump, masses 130 and 134 were measured on AX and H1. Then, after a final magnetic jump, masses 129 and 131 were measured on L1 and AX.

Table D.1
Isotopic composition of atmospheric Xe assumed for XeStd calibration. From <https://en.wikipedia.org/wiki/Isotopes_of_xenon>.

Isotope	Abundance
^{124}Xe	0.095%
^{126}Xe	0.089%
^{128}Xe	1.910%
^{129}Xe	26.401%
^{130}Xe	4.071%
^{131}Xe	21.232%
^{132}Xe	26.909%
^{134}Xe	10.436%
^{136}Xe	8.857%

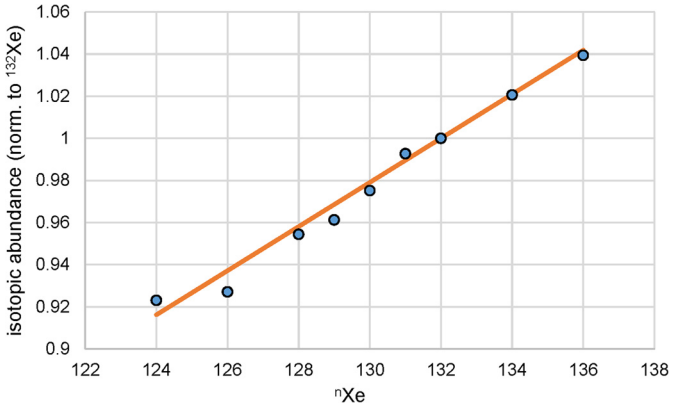

Fig. D.1. ^{132}Xe normalized and air standard normalized signal from XeStd (blue symbols), and the best-fit mass fractionation line (orange) of -1.047% per AMU used to estimate the isotopic composition of XeStd.

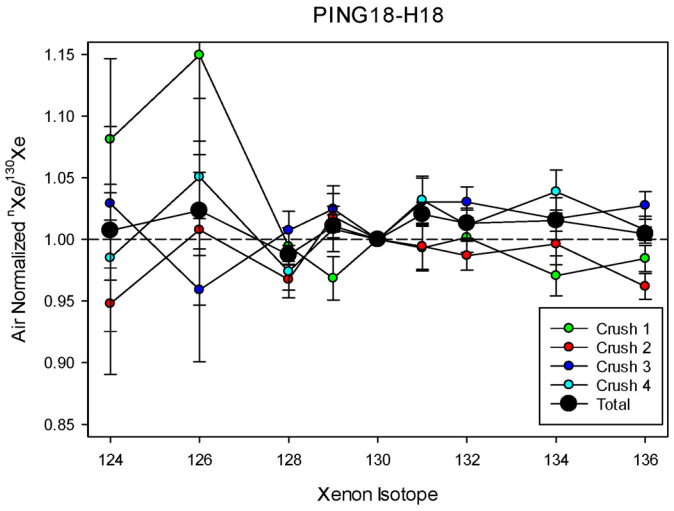

Fig. D.2. ^{130}Xe and air-normalized Xe isotope ratios measured on PING18-H18. Error bars are 1σ.

Sample

4.79 g of olivine from the >1 mm size fraction of sample PING18-H18 was sequentially crushed under vacuum, as described

Table D.2
Calibrated composition and current delivery of XeStd.

Overall	Total Xe (pcc)								
	16.69								
	124	126	128	129	130	131	132	134	136
XeStd pcc	0.01454	0.01396	0.30669	4.28879	0.66897	3.52881	4.52286	1.79326	1.55519
±	0.00009	0.00006	0.00090	0.00931	0.00096	0.00250	0.00000	0.00245	0.00417
± %	0.00615	0.00450	0.00293	0.00217	0.00143	0.00071	0.00000	0.00137	0.00268
XeStd Fractional	0.00087	0.00084	0.01837	0.25692	0.04007	0.21139	0.27094	0.10743	0.09316
Air Fractional	0.00095	0.00089	0.01910	0.26401	0.04071	0.21232	0.26909	0.10436	0.08857

Table D.3
Xenon isotopic concentrations and isotopic ratios measured on PING18-H18 in a 4-step crushing experiment.

		124Xe	126Xe	128Xe	129Xe	130Xe	131Xe	132Xe	134Xe	136Xe
Line Blank	*pcc*	1.29E-05	1.91E-05	4.99E-04	2.07E-03	2.78E-04	1.76E-03	1.55E-03	6.12E-04	5.01E-04
	± σ	5.17E-06	9.41E-06	1.80E-05	3.93E-04	4.27E-05	3.43E-04	9.62E-05	8.48E-05	4.39E-05
Crsh Blank	*pcc*	4.28E-05	2.99E-05	7.06E-04	9.89E-03	1.41E-03	7.29E-03	9.88E-03	3.95E-03	3.01E-03
	± σ	2.57E-06	1.79E-06	9.00E-06	1.60E-04	1.50E-05	1.23E-04	8.38E-05	5.72E-05	2.04E-05
Ping18 H18 Crush										
1: 2 min	*pcc*	1.61E-04	1.60E-04	2.98E-03	4.01E-02	6.38E-03	3.31E-02	4.23E-02	1.59E-02	1.37E-02
	± σ	9.66E-06	9.63E-06	3.80E-05	6.50E-04	6.79E-05	5.59E-04	3.59E-04	2.30E-04	9.24E-05
2: 2 min	*pcc*	1.75E-04	1.75E-04	3.60E-03	5.24E-02	7.93E-03	4.11E-02	5.17E-02	2.03E-02	1.66E-02
	± σ	1.05E-05	1.05E-05	4.59E-05	8.50E-04	8.44E-05	6.95E-04	4.39E-04	2.93E-04	1.12E-04
3: 5 min	*pcc*	4.32E-04	3.77E-04	8.50E-03	1.19E-01	1.80E-02	9.66E-02	1.22E-01	4.69E-02	4.02E-02
	± σ	2.59E-05	2.26E-05	1.08E-04	1.94E-03	1.91E-04	1.63E-03	1.04E-03	6.79E-04	2.72E-04
4: 10 min	*pcc*	4.05E-04	4.04E-04	8.04E-03	1.15E-01	1.76E-02	9.47E-02	1.18E-01	4.69E-02	3.86E-02
	± σ	2.43E-05	2.43E-05	1.03E-04	1.87E-03	1.87E-04	1.60E-03	9.99E-04	6.79E-04	2.61E-04
Total	*pcc*	**1.17E-03**	**1.12E-03**	**2.31E-02**	**3.27E-01**	**4.99E-02**	**2.66E-01**	**3.34E-01**	**1.30E-01**	**1.09E-01**
	± σ	**7.04E-05**	**6.70E-05**	**2.95E-04**	**5.30E-03**	**5.31E-04**	**4.49E-03**	**2.84E-03**	**1.88E-03**	**7.37E-04**
	Air Normalized									
1: 2 min	*nXe/130Xe*	1.0812	1.1495	0.9943	0.9684	1.0000	0.9931	1.0016	0.9705	0.9845
	±σ	0.0655	0.0697	0.0152	0.0177		0.0188	0.0120	0.0163	0.0107
2: 2 min	*nXe/130Xe*	0.9478	1.0078	0.9674	1.0186	1.0000	0.9944	0.9869	0.9963	0.9618
	±σ	0.0574	0.0611	0.0148	0.0186		0.0188	0.0118	0.0167	0.0104
3: 5 min	*nXe/130Xe*	1.0292	0.9590	1.0074	1.0247	1.0000	1.0304	1.0303	1.0169	1.0275
	±σ	0.0624	0.0581	0.0154	0.0188		0.0195	0.0124	0.0171	0.0111
4: 10 min	*nXe/130Xe*	0.9850	1.0507	0.9739	1.0084	1.0000	1.0319	1.0117	1.0387	1.0078
	±σ	0.0597	0.0637	0.0149	0.0185		0.0195	0.0121	0.0174	0.0109
Total	*nXe/130Xe*	**1.0073**	**1.0235**	**0.9875**	**1.0108**	**1.0000**	**1.0205**	**1.0132**	**1.0154**	**1.0046**
	±σ	**0.0305**	**0.0310**	**0.0076**	**0.0092**		**0.0096**	**0.0122**	**0.0085**	**0.0054**

below. The olivine separate was loaded in a hopper assembly located directly above a magnetically levitated stainless-steel slug in a vacuum chamber. The sample, hopper, and crusher were pumped to UHV with a turbomolecular pump, and baked at ~150 °C for three weeks. The crusher slug can be activated and degassed prior to sample crushing; the slug was degassed for 30 min immediately prior to the start of the crush analysis. A crush blank was measured, after which the sample was dumped from the hopper into the crusher. The sample was crushed in four separate steps of duration indicated in Table D.3. The crush blank obtained just prior to sample crushing is also indicated in the table. Analyses are corrected for line blanks but not for the crush blank based on the assumption that the crush blank is isotopically air-like and simply contributes to the air-contamination inherent to the sample.

Results

Results are listed in Table D.3. For the total sample, none of the crush steps yielded anomalous air-normalized $^{n}Xe/^{130}Xe$ ratios beyond 2σ uncertainty. In particular, the key radiogenic isotope ratios ($^{129}Xe/^{130}Xe$, $^{134}Xe/^{130}Xe$, and $^{136}Xe/^{130}Xe$) deviate from the atmospheric ratios by less than 1.5%. None of the individual crush steps yield compelling evidence for anomalous Xe isotope ratios either.

The total amount of ^{132}Xe extracted from the sample was 0.33 pcc/g. This concentration is substantially lower than measured in gas-rich MORB and back-arc glasses, subglacial Icelandic glass, and in ultramafic xenoliths.

Combining the total crush data for Xe with the total crush He-Ne-Ar data reported in the main text, the $^{3}He/^{130}Xe$ ratio of PING18-H18 is ~62. According to Mukhopadhyay (2012) Fig. 3, at this $^{3}He/^{130}Xe$ ratio, both MORB popping rock and the Iceland subglacial glass DICE10 have isotopic compositions (e.g., $^{129}Xe/^{130}Xe$) very close to atmospheric. Thus, the absence of a measured anomaly is not unexpected based on previous work, and may be interpreted simply as air contamination of sufficient magnitude to preclude detection of anomalous Baffin Island xenon.

References

Allègre, C.J., Staudacher, T., Sarda, P., Kurz, M., 1983. Constraints on evolution of Earth's mantle from rare gas systematics. Nature 303, 762–766.

Blundy, J., Wood, B., 2003. Mineral-melt partitioning of uranium, thorium and their daughters. Rev. Mineral. Geochem. 52, 59–123.

Bouhifd, M.A., Jephcoat, A.P., Porcelli, D., Kelley, S.P., Marty, B., 2020. Potential of Earth's core as a reservoir for noble gases: case for helium and neon. Geochem. Perspect. Lett., 15–18.

Clarke, D.B., 1968. Tertiary Basalts of the Baffin Bay Area.

Dixon, E.T., Honda, M., McDougall, I., Campbell, I.H., Sigurdsson, I., 2000. Preservation of near-solar neon isotopic ratios in Icelandic basalts. Earth Planet. Sci. Lett. 180, 309–324.

Dygert, N., Jackson, C.R., Hesse, M.A., Tremblay, M.M., Shuster, D.L., Gu, J.T., 2018. Plate tectonic cycling modulates Earth's 3He/22Ne ratio. Earth Planet. Sci. Lett. 498, 309–321.

Farley, K.A., Craig, H., 1994. Atmospheric argon contamination of ocean island basalt olivine phenocrysts. Geochim. Cosmochim. Acta 58, 2509–2517.

Farley, K.A., Neroda, E., 1998. Noble gases in the Earth's mantle. Annu. Rev. Earth Planet. Sci. 26, 189–218.

Forsyth, D.A., Morel-AL'Huissier, P., Asudeh, I., Green, A.G., 1986. Alpha Ridge and iceland-products of the same plume? J. Geodyn. 6, 197–214.

Füri, E., Hilton, D.R., Halldórsson, S.A., Barry, P.H., Hahm, D., Fischer, T.P., Grönvold, K., 2010. Apparent decoupling of the He and Ne isotope systematics of the Icelandic mantle: the role of He depletion, melt mixing, degassing fractionation and air interaction. Geochim. Cosmochim. Acta 74, 3307–3332.

Hansen, H., Nielsen, T.F., 1999. Crustal contamination in Palaeogene East Greenland flood basalts: plumbing system evolution during continental rifting. Chem. Geol. 157, 89–118.

Harrison, D., Burnard, P., Turner, G., 1999. Noble gas behaviour and composition in the mantle: constraints from the Iceland Plume. Earth Planet. Sci. Lett. 171, 199–207.

Heber, V.S., Baur, H., Bochsler, P., McKeegan, K.D., Neugebauer, M., Reisenfeld, D.B., Wieler, R., Wiens, R.C., 2012. Isotopic mass fractionation of solar wind: evidence from fast and slow solar wind collected by the Genesis mission. Astrophys. J. 759, 121.

Herzberg, C., Asimow, P.D., 2015. PRIMELT 3 MEGA. XLSM software for primary magma calculation: peridotite primary magma MgO contents from the liquidus to the solidus. Geochem. Geophys. Geosyst. 16, 563–578.

Honda, M., McDougall, I., Patterson, D.B., Doulgeris, A., Clague, D.A., 1993. Noble gases in submarine pillow basalt glasses from Loihi and Kilauea, Hawaii: a solar component in the Earth. Geochim. Cosmochim. Acta 57, 859–874. https://doi.org/10.1016/0016-7037(93)90174-U.

Horton, F., Farley, K., Jackson, M., 2019. Helium distributions in ocean island basalt olivines revealed by X-ray computed tomography and single-grain crushing experiments. Geochim. Cosmochim. Acta 244, 467–477.

Jackson, M.G., Carlson, R.W., Kurz, M.D., Kempton, P.D., Francis, D., Blusztajn, J., 2010. Evidence for the survival of the oldest terrestrial mantle reservoir. Nature 466, 853.

Jackson, M.G., Konter, J.G., Becker, T.W., 2017. Primordial helium entrained by the hottest mantle plumes. Nature 542, 340.

Jackson, M.G., Kurz, M.D., Hart, S.R., 2009. Helium and neon isotopes in phenocrysts from Samoan lavas: evidence for heterogeneity in the terrestrial high $^{3}He/^{4}He$ mantle. Earth Planet. Sci. Lett. 287 (3-4), 519–528.

Jackson, M.G., Kurz, M.D., Hart, S.R., Workman, R.K., 2007. New Samoan lavas from Ofu Island reveal a hemispherically heterogeneous high 3 He/4 He mantle. Earth Planet. Sci. Lett. 264, 360–374.

Jakobsson, M., Mayer, L., Coakley, B., Dowdeswell, J.A., Forbes, S., Fridman, B., Hodnesdal, H., Noormets, R., Pedersen, R., Rebesco, M., 2012. The international bathymetric chart of the Arctic Ocean (IBCAO) version 3.0. Geophys. Res. Lett. 39.

Jambon, A., Weber, H., Braun, O., 1986. Solubility of He, Ne, Ar, Kr and Xe in a basalt melt in the range 1250–1600 C. Geochemical implications. Geochim. Cosmochim. Acta 50, 401–408.

Kent, A.J.R., Stolper, E.M., Francis, D., Woodhead, J., Frei, R., Eiler, J., 2004. Mantle heterogeneity during the formation of the North Atlantic igneous province: constraints from trace element and Sr-Nd-Os-O isotope systematics of Baffin Island picrites. Geochem. Geophys. Geosyst. 5.

Kurz, M.D., Curtice, J., Fornari, D., Geist, D., Moreira, M., 2009. Primitive neon from the center of the Galápagos hotspot. Earth Planet. Sci. Lett. 286, 23–34.

Kurz, M.D., Jenkins, W.J., Hart, S.R., Clague, D., 1983. Helium isotopic variations in volcanic rocks from Loihi Seamount and the Island of Hawaii. Earth Planet. Sci. Lett. 66, 388–406.

Kurz, M.D., Moreira, M., Curtice, J., Lott III, D.E., Mahoney, J.J., Sinton, J.M., 2005. Correlated helium, neon, and melt production on the super-fast spreading East Pacific Rise near 17 S. Earth Planet. Sci. Lett. 232, 125–142.

Lass-Evans, S., 2004. The anatomy of the ancestral Iceland plume: a chemical and isotopic study of the Tertiary basalts and picrites from Baffin Island. PhD Thesis. University of Edinburgh.

Lawver, L.A., Müller, R.D., 1994. Iceland hotspot track. Geology 22, 311–314.

Lux, G., 1987. The behavior of noble gases in silicate liquids: solution, diffusion, bubbles and surface effects, with applications to natural samples. Geochim. Cosmochim. Acta 51, 1549–1560. https://doi.org/10.1016/0016-7037(87)90336-X.

Manglik, A., Christensen, U.R., 2006. Effect of lithospheric root on decompression melting in plume–lithosphere interaction models. Geophys. J. Int. 164, 259–270.

Marty, B., Tolstikhin, I., Kamensky, I.L., Nivin, V., Balaganskaya, E., Zimmermann, J.-L., 1998. Plume-derived rare gases in 380 Ma carbonatites from the Kola region (Russia) and the argon isotopic composition in the deep mantle. Earth Planet. Sci. Lett. 164, 179–192.

Moreira, M., Breddam, K., Curtice, J., Kurz, M.D., 2001. Solar neon in the Icelandic mantle: new evidence for an undegassed lower mantle. Earth Planet. Sci. Lett. 185, 15–23.

Moreira, M., Charnoz, S., 2016. The origin of the neon isotopes in chondrites and on Earth. Earth Planet. Sci. Lett. 433, 249–256.

Moreira, M., Kunz, J., Allegre, C., 1998. Rare gas systematics in popping rock: isotopic and elemental compositions in the upper mantle. Science 279, 1178–1181.

Mukhopadhyay, S., 2012. Early differentiation and volatile accretion recorded in deep-mantle neon and xenon. Nature 486, 101–104.

Mundl-Petermeier, A., Walker, R.J., Jackson, M.G., Blichert-Toft, J., Kurz, M.D., Halldórsson, S.A., 2019. Temporal evolution of primordial tungsten-182 and 3He/4He signatures in the Iceland mantle plume. Chem. Geol. 525, 245–259.

Nielsen, T.K., Larsen, H.C., Hopper, J.R., 2002. Contrasting rifted margin styles south of Greenland: implications for mantle plume dynamics. Earth Planet. Sci. Lett. 200, 271–286.

Oakey, G.N., Chalmers, J.A., 2012. A new model for the Paleogene motion of Greenland relative to North America: plate reconstructions of the Davis Strait and Nares Strait regions between Canada and Greenland. J. Geophys. Res., Solid Earth 117.

Péron, S., Moreira, M., Agranier, A., 2018. Origin of light noble gases (He, Ne, and Ar) on Earth: a review. Geochem. Geophys. Geosyst. 19, 979–996. https://doi.org/10.1002/2017GC007388.

Péron, S., Moreira, M., Colin, A., Arbaret, L., Putlitz, B., Kurz, M.D., 2016. Neon isotopic composition of the mantle constrained by single vesicle analyses. Earth Planet. Sci. Lett. 449, 145–154. https://doi.org/10.1016/j.epsl.2016.05.052.

Porcelli, D., Halliday, A.N., 2001. The core as a possible source of mantle helium. Earth Planet. Sci. Lett. 192, 45–56. https://doi.org/10.1016/S0012-821X(01)00418-6.

Poreda, R.J., Farley, K.A., 1992. Rare gases in Samoan xenoliths. Earth Planet. Sci. Lett. 113, 129–144.

Raquin, A., Moreira, M.A., Guillon, F., 2008. He, Ne and Ar systematics in single vesicles: mantle isotopic ratios and origin of the air component in basaltic glasses. Earth Planet. Sci. Lett. 274, 142–150.

Rizo, H., Walker, R.J., Carlson, R.W., Horan, M.F., Mukhopadhyay, S., Manthos, V., Francis, D., Jackson, M.G., 2016. Preservation of Earth-forming events in the tungsten isotopic composition of modern flood basalts. Science 352, 809–812.

Robillard, I., Francis, D., Ludden, J.N., 1992. The relationship between E- and N-type magmas in the Baffin Bay lavas. Contrib. Mineral. Petrol. 112, 230–241.

Saunders, A.D., Fitton, J.G., Kerr, A.C., Norry, M.J., Kent, R.W., 1997. The north Atlantic igneous province. Geophys. Monogr. - Am. Geophys. Union 100, 45–94.

Starkey, N.A., Stuart, F.M., Ellam, R.M., Fitton, J.G., Basu, S., Larsen, L.M., 2009. Helium isotopes in early Iceland plume picrites: constraints on the composition of high 3He/4He mantle. Earth Planet. Sci. Lett. 277, 91–100.

Staudacher, T., Sarda, P., Allègre, C.J., 1990. Noble gas systematics of Réunion island, Indian Ocean. Chem. Geol. 89, 1–17.

Steinberger, B., Bredow, E., Lebedev, S., Schaeffer, A., Torsvik, T.H., 2019. Widespread volcanism in the Greenland–North Atlantic region explained by the Iceland plume. Nat. Geosci. 12, 61–68.

Storey, M., Duncan, R.A., Pedersen, A.K., Larsen, L.M., Larsen, H.C., 1998. 40Ar/39Ar geochronology of the West Greenland Tertiary volcanic province. Earth Planet. Sci. Lett. 160, 569–586.

Stuart, F.M., Lass-Evans, S., Fitton, J.G., Ellam, R.M., 2003. High 3 He/4 He ratios in picritic basalts from Baffin Island and the role of a mixed reservoir in mantle plumes. Nature 424, 57.

Sumino, H., Kaneoka, I., Matsufuji, K., Sobolev, A.V., 2006. Deep mantle origin of kimberlite magmas revealed by neon isotopes. Geophys. Res. Lett. 33.

Torsvik, T.H., Amundsen, H.E., Trønnes, R.G., Doubrovine, P.V., Gaina, C., Kusznir, N.J., Steinberger, B., Corfu, F., Ashwal, L.D., Griffin, W.L., 2015. Continental crust beneath southeast Iceland. Proc. Natl. Acad. Sci. 112, E1818–E1827.

Tucker, J.M., Mukhopadhyay, S., 2014. Evidence for multiple magma ocean outgassing and atmospheric loss episodes from mantle noble gases. Earth Planet. Sci. Lett. 393, 254–265.

Tucker, J.M., Mukhopadhyay, S., Gonnermann, H.M., 2018. Reconstructing mantle carbon and noble gas contents from degassed mid-ocean ridge basalts. Earth Planet. Sci. Lett. 496, 108–119. https://doi.org/10.1016/j.epsl.2018.05.024.

Valbracht, P.J., Staudacher, T., Malahoff, A., Allègre, C.J., 1997. Noble gas systematics of deep rift zone glasses from Loihi Seamount, Hawaii. Earth Planet. Sci. Lett. 150, 399–411. https://doi.org/10.1016/S0012-821X(97)00094-0.

White, R., McKenzie, D., 1989. Magmatism at rift zones: the generation of volcanic continental margins and flood basalts. J. Geophys. Res., Solid Earth 94, 7685–7729.

Willhite, L.N., Jackson, M.G., Blichert-Toft, J., Bindeman, I., Kurz, M.D., Halldórsson, S.A., Harðardóttir, S., Gazel, E., Price, A.A., Byerly, B.L., 2019. Hot and heterogenous high-3He/4He components: new constraints from proto-Iceland plume lavas from Baffin Island. Geochem. Geophys. Geosyst.

Yokochi, R., Marty, B., 2004. A determination of the neon isotopic composition of the deep mantle. Earth Planet. Sci. Lett. 225, 77–88.